

Engineering metal-nanoantennae/dye complexes for maximum fluorescence enhancement

Xiang Meng,^{1,*} Richard R. Grote,¹ Jerry I Dadap,²
Nicolae C. Panoiu,³ and Richard M. Osgood, Jr.^{1,2}

¹*Department of Electrical Engineering, Columbia University,
New York, New York 10027, USA*

²*Department of Applied Physics and Applied Mathematics, Columbia University
New York, New York 10027, USA*

³*Department of Electronic and Electrical Engineering, University College London
Torrington Place, London WC1E 7JE, UK*

*meng@ee.columbia.edu

Abstract: We theoretically investigate the fluorescence enhancement of a molecule placed in a variable (4 - 20 nm) gap of a plasmonic dimer, with different dye molecules as well as different nanoparticle geometries, using a fully vectorial three-dimensional finite-difference time-domain (3D FDTD) method. This work extends previous studies on molecular fluorescence in the vicinity of metal interfaces and single nanoparticles and shows how the radiative emission of a molecule can be further enhanced by engineering the geometry of a plasmonic structure. Through the use of rigorous 3D FDTD calculations, in conjunction with analytic guidance based on temporal coupled-mode (TCM) theory, we develop a design procedure for antennae assemblies that is useful both for general understanding of molecule-metal structure interaction and experimental efforts in plasmon-enhanced molecular spectroscopy.

© 2014 Optical Society of America

OCIS codes: (240.6680) Surface plasmons; (280.4788) Optical sensing and sensors; (260.2510) Fluorescence.

References and links

1. J. A. Schuller, E. S. Barnard, W. Cai, Y. C. Jun, J. S. White, and M. L. Brongersma, "Plasmonics for extreme light concentration and manipulation," *Nature Mater.* **9**, 193–204 (2010).
2. P. Bharadwaj, B. Deutsch, and L. Novotny, "Optical antennas," *Adv. Opt. Photon.* **1**, 438–483 (2009).
3. X. Jiao and S. Blair, "Optical antenna design for fluorescence enhancement in the ultraviolet," *Opt. Express* **20**, 29909–29922 (2012).
4. B. B. Yousif and A. S. Samra, "Optical responses of plasmonic gold nanoantennas through numerical simulation," *J. Nanopart. Res.* **15**, 1–15 (2013).
5. X. Meng, R. R. Grote, and R. M. Osgood, "Engineering 3d metal nanoantenna for fluorescence enhancement," in "CLEO: Applications and Technology," (Optical Society of America, 2013), pp. JT4A–55.
6. C. Forestiere, A. Handin, and L. Dal Negro, "Enhancement of molecular fluorescence in the uv spectral range using aluminum nanoantennas," *Plasmonics* pp. 1–11 (2014).
7. M. Quinten, *Optical Properties of Nanoparticle Systems: Mie and Beyond* (Wiley-Vch, 2010).
8. P. Anger, P. Bharadwaj, and L. Novotny, "Enhancement and quenching of single-molecule fluorescence," *Phys. Rev. Lett.* **96**, 113002 (2006).
9. S. Kühn, U. Håkanson, L. Rogobete, and V. Sandoghdar, "Enhancement of single-molecule fluorescence using a gold nanoparticle as an optical nanoantenna," *Phys. Rev. Lett.* **97**, 017402 (2006).
10. L. Novotny and B. Hecht, *Principles of Nano-optics* (Cambridge university press, 2006).

11. D. Nykypanchuk, M. M. Maye, D. van der Lelie, and O. Gang, "Dna-guided crystallization of colloidal nanoparticles," *Nature (London)* **451**, 549–552 (2008).
12. M. M. Maye, M. T. Kumara, D. Nykypanchuk, W. B. Sherman, and O. Gang, "Switching binary states of nanoparticle superlattices and dimer clusters by dna strands," *Nature Nanotech.* **5**, 116–120 (2009).
13. H. Xiong, M. Y. Sfeir, and O. Gang, "Assembly, structure and optical response of three-dimensional dynamically tunable multicomponent superlattices," *Nano Lett.* **10**, 4456–4462 (2010).
14. S. Zhang, J. Zhou, Y.-S. Park, J. Rho, R. Singh, S. Nam, A. K. Azad, H.-T. Chen, X. Yin, A. J. Taylor *et al.*, "Photoinduced handedness switching in terahertz chiral metamolecules," *Nat. Commun.* **3**, 942 (2012).
15. L. Huang, X. Chen, B. Bai, Q. Tan, G. Jin, T. Zentgraf, and S. Zhang, "Helicity dependent directional surface plasmon polariton excitation using a metasurface with interfacial phase discontinuity," *Light Sci. Appl.* **2**, e70 (2013).
16. H. A. Haus, *Waves and fields in optoelectronics* (Prentice-Hall Englewood Cliffs, NJ, 1984).
17. R. L. Olmon, P. M. Krenz, A. C. Jones, G. D. Boreman, and M. B. Raschke, "Near-field imaging of optical antenna modes in the mid-infrared," *Opt. Express* **16**, 20295–20305 (2008).
18. A. C. Jones, R. L. Olmon, S. E. Skrabalak, B. J. Wiley, Y. N. Xia, and M. B. Raschke, "Mid-ir plasmonics: near-field imaging of coherent plasmon modes of silver nanowires," *Nano Lett.* **9**, 2553–2558 (2009).
19. J. R. Lakowicz, "Plasmonics in biology and plasmon-controlled fluorescence," *Plasmonics* **1**, 5–33 (2006).
20. X. Huang, P. K. Jain, I. H. El-Sayed, and M. A. El-Sayed, "Plasmonic photothermal therapy (pptt) using gold nanoparticles," *Laser Med. Sci.* **23**, 217–228 (2008).
21. L. Novotny and N. van Hulst, "Antennas for light," *Nature Photon.* **5**, 83–90 (2011).
22. C. Min and G. Veronis, "Absorption switches in metal-dielectric-metal plasmonic waveguides," *Opt. Express* **17**, 10757–10766 (2009).
23. V. Valev, N. Smisdom, A. Silhanek, B. De Clercq, W. Gillijns, M. Ameloot, V. Moshchalkov, and T. Verbiest, "Plasmonic ratchet wheels: switching circular dichroism by arranging chiral nanostructures," *Nano Lett.* **9**, 3945–3948 (2009).
24. M. J. Huttunen, G. Bautista, M. Decker, S. Linden, M. Wegener, and M. Kauranen, "Nonlinear chiral imaging of subwavelength-sized twisted-cross gold nanodimers [invited]," *Opt. Mater. Express* **1**, 46–56 (2011).
25. J. Gersten and A. Nitzan, "Spectroscopic properties of molecules interacting with small dielectric particles," *J. Chem. Phys.* **75**, 1139–1152 (1981).
26. P. Bharadwaj, L. Novotny *et al.*, "Spectral dependence of single molecule fluorescence enhancement," *Opt. Express* **15**, 14266–14274 (2007).
27. E. N. Economou, *Green's Functions in Quantum Physics*, vol. 3 (Springer, 1984).
28. A. D. Rakic, A. B. Djurišić, J. M. Elazar, and M. L. Majewski, "Optical properties of metallic films for vertical-cavity optoelectronic devices," *Appl. Opt.* **37**, 5271–5283 (1998).
29. G. Veronis and S. Fan, "Overview of simulation techniques for plasmonic devices," in "Surface plasmon nanophotonics," (Springer, 2007), pp. 169–182.
30. C. Dyes, "Biotium inc." <http://www.biotium.com/> (2013).
31. J. B. Khurgin, G. Sun, and R. Soref, "Practical limits of absorption enhancement near metal nanoparticles," *Appl. Phys. Lett.* **94**, 071103–071103 (2009).
32. J. B. Khurgin, G. Sun, and R. Soref, "Electroluminescence efficiency enhancement using metal nanoparticles," *Appl. Phys. Lett.* **93**, 021120–021120 (2008).
33. J. D. Jackson and R. F. Fox, "Classical electrodynamics," *Am. J. Phys.* **67**, 841 (1999).
34. J. Dadap, J. Shan, K. Eisenthal, and T. Heinz, "Second-harmonic rayleigh scattering from a sphere of centrosymmetric material," *Phys. Rev. Lett.* **83**, 4045–4048 (1999).
35. S. Oldenburg, R. Averitt, S. Westcott, and N. Halas, "Nanoengineering of optical resonances," *Chem. Phys. Lett.* **288**, 243–247 (1998).
36. B. Willingham, D. Brandl, and P. Nordlander, "Plasmon hybridization in nanorod dimers," *Appl. Phys. B* **93**, 209–216 (2008).
37. N. J. Halas, S. Lal, W.-S. Chang, S. Link, and P. Nordlander, "Plasmons in strongly coupled metallic nanostructures," *Chem. Rev.* **111**, 3913–3961 (2011).
38. D. Y. Lei, A. Aubry, Y. Luo, S. A. Maier, and J. B. Pendry, "Plasmonic interaction between overlapping nanowires," *ACS Nano.* **5**, 597–607 (2010).
39. C. F. Bohren and D. R. Huffman, *Absorption and Scattering of Light by Small Particles* (Wiley.com, 2008).
40. P. Zijlstra, J. W. Chon, and M. Gu, "Five-dimensional optical recording mediated by surface plasmons in gold nanorods," *Nature (London)* **459**, 410–413 (2009).
41. M. Rang, A. C. Jones, F. Zhou, Z.-Y. Li, B. J. Wiley, Y. Xia, and M. B. Raschke, "Optical near-field mapping of plasmonic nanoprisms," *Nano Lett.* **8**, 3357–3363 (2008).
42. A. Kinkhabwala, Z. Yu, S. Fan, Y. Avlasevich, K. Müllen, and W. Moerner, "Large single-molecule fluorescence enhancements produced by a bowtie nanoantenna," *Nature Photon.* **3**, 654–657 (2009).

1. Introduction

It is well known that the absorption cross section and radiative efficiency of a molecule can be enhanced by a nearby plasmonic nanostructure; this enhancement is important, for example, for applications in biosensing and photovoltaics [1, 2]. Furthermore, while the enhancement of the local optical field due to the metal structure can be calculated accurately numerically, much less numerical research has been carried out on the *combined effects* of excitation and quenching. Fluorescence enhancement depends on the metallic composition, size, shape, orientation of the nanoantennae, the dielectric properties of the surrounding medium, the number of nanoantennae, and the polarization state and frequency of the incident beam. Each of these parameters modifies the combined effects of excitation by the incident field and ohmic loss in the nanoantennae [3–5]. Recently, Dal Negro and coworkers have theoretically investigated the fluorescence enhancement based on varying shapes and sizes of single metal nanoparticle, as well as their near-field interactions in the deep-ultraviolet spectral range using a surface integral equation method [6]. However, there has been no systematic investigation of the emission properties of dye coupled to nanoantennae of different shapes, sizes and their interactions in the visible spectrum region.

Analysis of the fluorescence properties of an emitter such as a dye molecule can be carried out by generalized Mie theory (GMT) [7]. However, Mie theory cannot directly predict the scattering of non-spherical particles or of an arbitrary ensemble of nanoparticles. Thus for the case of light scattering by non-spherical nanoparticles, only approximate GMT algorithms have been established. In addition, an important earlier analytic study, which considered a single spherical antenna [8–10], used a Green's function approach to analyze the molecule's linear excitation rate. This method provided a useful analytic formulation; however, such an approach may lack the generality of rigorous numerical computation.

Concomitantly, synthesis methods have been developed by many groups, which enable fabrication of specific nanoparticle structures for fluorescence with sub-nanometer precisions using DNA self-assembly. For example, Gang and coworkers have developed methods of fabricating arrays by DNA self-assembly [11–13]. These arrays consist of structures formed with metal nanoparticles and dye molecules. In addition, Zhang and coworkers also have implemented several viable synthetic methodologies for the fabrication of a range of nanoscale formulations [14, 15]. These synthesis methods require a companion approach for computing the optical/fluorescence properties of the structures.

In this paper, we use a method based on full vectorial three-dimensional finite-difference time-domain (3D FDTD) computation to achieve accurate fluorescence enhancement calculations for arbitrary-shaped metal nanoparticle antennae. In addition, we show that temporal coupled-mode (TCM) theory [16] can be used for analytical guidance in the optimization of the antennae design. We have obtained the antennae configurations for the optimized fluorescence enhancement of each of a selected set of dye molecules, which are matched to three different antennae geometries. Our results provide guidance for the rational design of optimized metallic nanoparticle complexes for maximum fluorescence enhancement. Finally, we note that this approach provides a design method for applications of optically active nanostructures in near-field imaging [17, 18], biosensing [19, 20], light harvesting [21, 22] and nonlinear optical properties of metal nanostructures [23, 24].

2. Dye-molecule/antenna complex

First, for our emitter-dye complexes, the emission spectrum of each dye is dependent on both the spectral response of each dye and the response and efficiency of its nearby nanoantenna. Second, each dye/antenna combination exhibits strong fluorescence enhancement only over a limited spectral region, where in this paper, only antennae having a fixed specific volume of

metal are considered and compared. This behavior is sketched notionally in Fig. 1(a) for the cases of a spherical- and an ellipsoidal-dimer antenna. This spectral response can be broadened or shifted by changes in the geometry of the antenna. For example, a change in the spacing between the antenna nanoparticles shifts the antenna response - but only by a relatively small amount; see the dotted line in Fig. 1(a). On the other hand, it is possible to access other spectral regions using an antenna with a different geometrical shape such as the ellipsoid shown in Fig. 1(a), since the antenna has a distinct, shape-dependent localized-plasmon resonance frequency. Finally, note that enlarging the radius of a spherical dimer also shifts the antenna response, while at the same time increasing the magnitude of field enhancement due to its larger antenna polarizability [Fig. 1(b)]. However, larger antennae also experience larger ohmic loss. This large ohmic loss makes the larger spherical dimer/dye cluster to be a less efficient emitter than the smaller ellipsoid dimer/dye cluster. Therefore, the scope of this paper focuses on investigating the influence of the nanoparticle geometry, rather than the dependence on volumetric scaling.

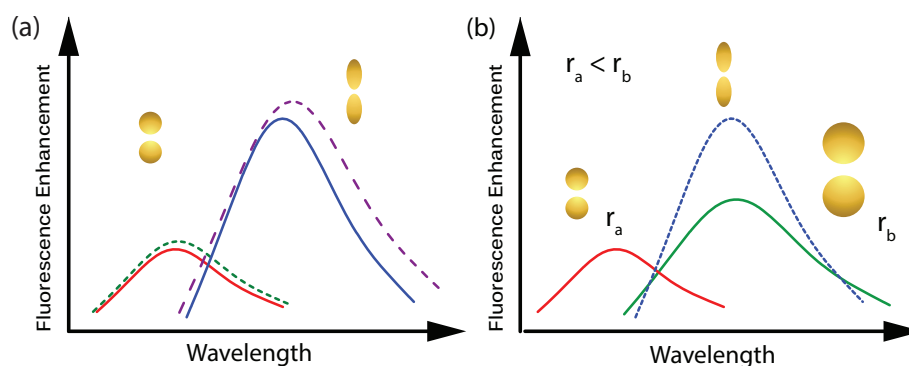


Fig. 1. (a) A conceptual or notional sketch showing how the choice of nanodimer type (a spherical and ellipsoidal dimer with a fixed volume are shown here) selectively enhances a certain fluorescence-emission wavelength region. Only a very limited tuning of the dimers spectral response is achieved by changes in the interdimer-nanoparticle spacing. For example, when the dimer spacing is adjusted by 1nm, the resonance will shift from solid curve to dash line. (b) Spectral shifting and variation in fluorescence enhancement can also be achieved with a change in dimer radius (solid lines). The larger enhancement due to shape effect is shown for comparison (dotted lines).

Our goal is to provide a general approach to designing nanoantenna for efficient molecule light-emitting clusters. Thus, we consider the radiative and quenching processes of an excited emitting dye molecule in the near field of a metal nanoantennae, which is illuminated by a monochromatic optical source, as shown in Fig. 2(a). The dye molecule is approximated, as shown in Fig. 2(b), by a two-level system. In the presence of incident light with intensity I_0 , the molecule undergoes optical excitation followed by either nonradiative quenching or fluorescence, with an appropriate Stokes shift. If a dye molecule is located within the near field of metal antenna, the existence of resonant localized plasmons within the metal can enhance these optical processes. In effect, the metal antennae causes a much stronger local field to form at the position of the dye molecules due to excitation of localized surface plasmons (LSP), which corresponds to the external field distribution, causing, in turn, stronger optical excitation of the dye molecules. This excited molecule gives enhanced fluorescence as it decays radiatively with rate $\gamma_{rad} = 1/\tau_{rad}$, as shown in Fig. 2(c). Note also that ohmic loss within the metal antenna also inserts an additional non-radiative channel with the non-radiative decay rate of $\gamma_{nr} = 1/\tau_{nr}$

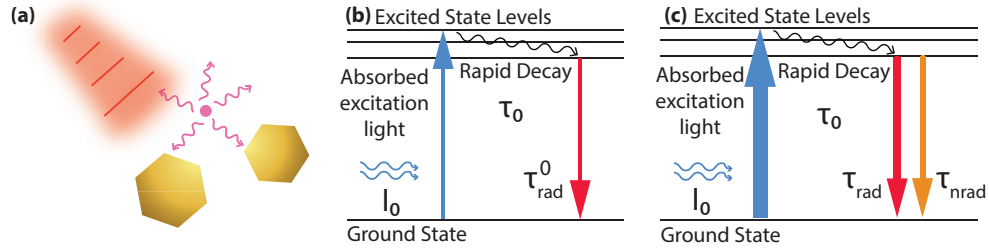


Fig. 2. (a) A schematic illustration of an antenna-dye system under laser illumination. (b) Two-level system for dye molecules in free space. (c) Two-level system for dye molecules near metallic nanoantennae.

that is not present in an isolated dye molecule.

Considering these processes, we can express the fluorescence rate γ_{em} of a single molecule as the product of an excitation rate γ_{exc} and the quantum yield q , where q is defined as the ratio of radiative transition rate (from excited to ground state) to the total decay rate: thus nonradiative quenching lowers q . It is sufficient to treat the excitation and emission processes independently because there is no coherence between the two processes [8]. The fluorescence enhancement can then be expressed as

$$\frac{\gamma_{em}}{\gamma_{em}^0} = \frac{\gamma_{exc}}{\gamma_{exc}^0} \cdot \frac{q}{q^0} \quad (1)$$

where the superscript '0' indicates the corresponding free-space quantity. Since we are considering only linear excitation processes, the excitation rate of the molecule is directly proportional to the number of incident photons, i.e., the incident intensity of the field:

$$\frac{\gamma_{exc}}{\gamma_{exc}^0} = \frac{|\mathbf{E}(\mathbf{r})|^2}{|\mathbf{E}_0(\mathbf{r})|^2} \quad (2)$$

The values of $\mathbf{E}(\mathbf{r})$ and $\mathbf{E}_0(\mathbf{r})$, which are the electric-field strengths for a specific optical frequency ω at the location, \mathbf{r} , of the molecule with and without the presence of an antenna, are obtained from our 3D FDTD calculations. The fluorescence enhancement is calculated by approximating the emitting molecule as a classical dipole; this approach has been described earlier by Gersten and Nitzan [25] and Novotny [8, 9]. The wavelength of the dipole is set to the emission wavelength of the dye, i.e., the Stokes shift is empirically accounted for. To obtain the quantum yield, q , of the isolated molecule, ohmic loss must be obtained using the dielectric function of the nanoantenna metal. This process includes a nonradiative rate γ_{nrad} , which then gives the quantum yield [26],

$$q = \frac{\gamma_{rad}/\gamma_{rad}^0}{\gamma_{rad}/\gamma_{rad}^0 + \gamma_{nrad}/\gamma_{rad}^0 + (1 - q^0)/q^0} \quad (3)$$

where $\gamma_{rad}/\gamma_{rad}^0$ and $\gamma_{nrad}/\gamma_{rad}^0$ are normalized radiative and non-radiative decay rates and q^0 is the free-space intrinsic quantum yield of dye molecules. Placing the emitter within the near-field of the nanoantennae increases its local optical density of states [27]. Then based on Fermi's Golden rule, the radiative decay rate will change compared to its value in free space. The analysis - discussed in [8, 10] - shows that the normalized energy-transfer rate can be written as $\gamma_{rad}/\gamma_{rad}^0 = P_{rad}/P_0$ and $\gamma_{nrad}/\gamma_{rad}^0 = P_{nrad}/P_0$, with P_{rad} being the power radiated by the

classical dipole in the presence of a metal nanoparticle, P_{nrad} being the power absorbed by the metal particle due to ohmic loss, and P_0 being the power radiated by a classical dipole in free space. The quantum yield is then obtained by measuring the power absorbed by the nanoantenna and the power emitted from the dipole-nanoantenna system.

3. Theoretical approach

In order to model the metal antennae optical response accurately, a parameterized Drude-Lorentz model [28, 29] was used. The analysis below considers Au antennae because of the prevalence of Au antennae in many fluorescence applications [8, 11]. We chose dyes that emit at red or near-infrared wavelengths because Au has a low absorption coefficient in this wavelength range. In this work, the size effects on the metal dielectric constant were neglected and all dye-molecules are assumed to have unity intrinsic quantum yield, i.e. $q^0 = 1$. In addition, because they are commonly used in cellular and biophotonics applications, we chose commercially available fluorochrome conjugates for these molecules, namely, $CF^{TM}568$, $CF^{TM}660R$ and $CF^{TM}790$ [30], which have useful spectral distributions, namely excitation maxima at 562nm, 663nm, 784nm, and peak emission wavelengths at 583nm, 682nm, and 806nm, respectively.

3.1. Analytic method

In order to gain analytical insight into the optical properties of our nano-system, we first treat the metal nanoparticles as coupled resonators and employ the TCM theory discussed by Haus [16] to analyze the energy transfer between the incident light and metal nanospheres. While the use of the TCM theory is approximate, it does enable a qualitative analysis of our systems. It, thus, allows us to determine the factors controlling the antennae performance and provides guidance for understanding, under which conditions, the metal antennae will increase radiative efficiency. The framework of the TCM theory can be best illustrated by considering the fields of a metal antenna cluster in the presence of an exciting beam with power of $|s_+|^2$.

For illustrative purposes here, we consider a metal antenna consisting of two spheres with a fixed spacing, i.e., a dimer, which is illuminated by a beam propagating in a direction perpendicular to and the polarization paralleled to the dimer axis. The TCM theory then generates the following rate equations to describe the relationship between the isolated sphere LSP-modes, $a_{1,2}$ with energies $|a_1|^2$ and $|a_2|^2$ and LSP resonant frequency ω_1 and ω_2 ,

$$\frac{da_1}{dt} = i\omega_1 a_1 - \frac{\gamma_{nrad} + \gamma_{rad}}{2} a_1 + \kappa_{in} s_+ + \frac{\gamma_{12}}{2} a_2 \quad (4)$$

$$\frac{da_2}{dt} = i\omega_2 a_2 - \frac{\gamma_{nrad} + \gamma_{rad}}{2} a_2 + \kappa_{in} s_+ + \frac{\gamma_{21}}{2} a_1 \quad (5)$$

where γ_{rad} is the radiative decay rate of a sphere with radius of r_0 at frequency ω gives [31]

$$\gamma_{rad} = \gamma_{rad}^{A\pi} = \left(\frac{2\pi r_0}{\lambda} \right)^3 \frac{\omega}{1 + 2\epsilon_D} \quad (6)$$

and λ and ϵ_D are the wavelength of incident beam and the dielectric constant of the medium, respectively; the nonradiative decay rates $\gamma_{nrad} = \gamma$ with γ being the metal ohmic loss in the Lorentz-Drude approximation. The in-coupling coefficient, κ_{in} , is the degree of coupling between the power of incident light and the energy of LSP, and γ_{12} and γ_{21} are the coupling coefficients between an LSP of one sphere with another.

Based on the dipole-dipole approximation [31, 32], the in-coupling coefficient κ_{in} can be evaluated as $\kappa_{in} = (\gamma_{rad}^{\Omega})^{1/2}$, with Ω being the far-field solid angle, where $\gamma_{rad}^{\Omega} = \gamma_{rad} \int_0^{\Omega} f(\theta, \phi) d\Omega$ and $f(\theta, \phi) = 3(1 - \sin^2 \theta \cos^2 \phi)/8\pi$. Due to the symmetry of our dimer system, the coupling

coefficients $\gamma_{12} = \gamma_{21} = \gamma_c$ and the amplitudes of the LSP modes $a_1 = a_2 = a$. We can evaluate the γ_c using overlap integral as follows,

$$\gamma_c = \frac{\frac{\omega}{2} \epsilon_0 \int_{mode} [\epsilon(\mathbf{r}) - \epsilon_d] E_1^*(\mathbf{r}) \cdot E_2(\mathbf{r}) dV}{|a|^2} \quad (7)$$

where $E_1(\mathbf{r})$ is the electric field at location \mathbf{r} when both LSP_1 and LSP_2 are present, $E_2(\mathbf{r})$ is the electric field at location \mathbf{r} when only LSP_2 is present and the LSP mode energy $|a|^2 = \frac{1}{2} \epsilon_0 \epsilon_D E_{max}^2 V_{eff}$, where V_{eff} is the effective mode volume [31]. Therefore, the steady-state solution of Eqs. (4) and (5) yields

$$a = \frac{2\kappa_{in}}{(\gamma_{rad} + \gamma_{nrad} - \gamma_c) - 2j(\omega - \omega_0)} s_+, \quad (8)$$

where ω_0 is the LSP resonance frequency. This equation shows the proportionality between s_+ and a , and hence between the incident power $|E_{inc}|^2$ and the isolated LSP $|E_{max}|^2$ of the sphere. The radiative γ_{rad} and non-radiative loss rates γ_{nrad} are mostly dependent on the particle size, while the coupling rate γ_c is mostly dependent on the inter-particle spacing. By coupling power back and forth between the two resonators the total loss rate $\gamma_{rad} + \gamma_{nrad} - \gamma_c$ is actually reduced, hence the increase in intensity. We can then vary the enhancement via a change in ω or in nanoparticle geometry.

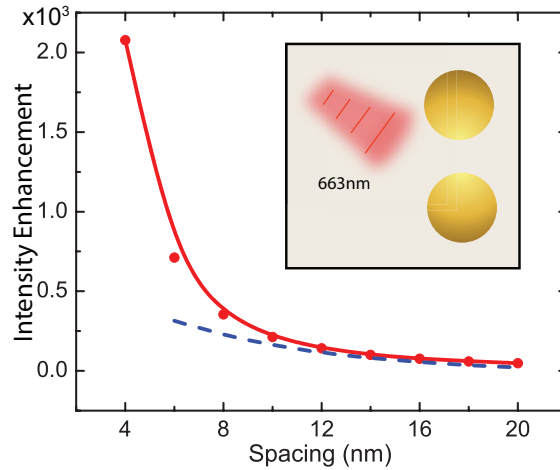


Fig. 3. The intensity enhancement measured at the center of the gap using TCM is presented as the dashed curve (blue) for a dimer structure with two 40nm-radius spherical Au particles under the illumination of 663nm light; the solid dot (red) is the result from FDTD simulations and the solid curve (red) is an interpolation based on FDTD results; note that the curves continue to diverge at smaller interatomic spacings of the dimer.

As mentioned before, while useful for qualitative insight, TCM is not as precise as is our numerical computation. Thus, we illustrate its accuracy with a detailed comparison between the results using TCM theory and FDTD simulation. This is shown in Fig. 3. For this comparison, we have selected a dimer structure with two 40nm-radius spherical Au particles under illumination by 663nm light. The surface-to-surface spacing is adjusted from 4nm to 20nm. The dashed line shows the enhancement achieved from using of TCM, which is in good agreement with the FDTD results (solid curve) at larger spacing (>10 nm). At this larger spacing, results obtained using an isolated metal-sphere-nanoparticle overlap equation, i.e., Eq. (7), agree well with the exact numerical solution.

3.2. Simulation

The advantages of FDTD simulation are its accuracy and simplification of implementation. Our simulations are implemented on the computer clusters (gen04) at Center for Functional Nanomaterials at Brookhaven National Laboratory. The problem was solved across hundreds of cores, which can not only divide a large numerical problem into smaller calculations, but also investigate multiple structures concurrently. Our code has been tested against analytical and experimental results [8] for the single-particle case and has been proven to yield the correct results (not shown). For our simulation model, a nanoantenna/dye molecule was illuminated using a *cw* plane-wave source, with an excitation wavelength located at the peak absorption frequency of the dye molecules. The dipole radiates at the Stokes-shifted emission frequency of the dye molecules. In FDTD, we surround the metal particles with a suitably chosen closed surface; we then calculate the net power flowing in through this closed surface, averaged over time. This averaged power into the closed surface is then the averaged power absorbed by the metal particles. A perfectly matched layer (PML) was used as the radiation boundary condition for the computational domain and the simulation had a mesh size of 0.5nm, which achieves results within 2% difference compared with that with a superfine/ultrahigh resolution i.e. a mesh size of 0.1nm.

4. Results

4.1. Spherical dimer

Calculations of the fluorescence enhancement and quenching of a single spherical metallic nanoantenna have been previously extensively investigated [2, 8, 26] yet it is useful to review briefly the fundamentals of this standard model system for an optical antennae photoresponse. For example, based on a quasi-static approximation [33], where the center of nanoparticle is located at the origin, the electric field near-field region due to a single spherical metallic nanoparticle is given as follows:

$$\mathbf{E}(r, \theta) = E_0(\cos\theta\mathbf{e}_r - \sin\theta\mathbf{e}_\theta) + \frac{\alpha(\omega) E_0}{4\pi\epsilon_0 r^3} (2\cos\theta\mathbf{e}_r + \sin\theta\mathbf{e}_\theta) \quad (9)$$

where \mathbf{e}_r and \mathbf{e}_θ are the unit vectors in radial and polar directions, respectively; $\alpha(\omega)$ denotes the polarizability of the metal particle and r is the distance from the center of particle. The general expression for polarizability of the metal sphere [34] is

$$\alpha(\omega) = 4\pi\epsilon_0 r_0^3 \frac{\epsilon_M(\omega) - \epsilon_D(\omega)}{\epsilon_M(\omega) + 2\epsilon_D(\omega)} \quad (10)$$

where ϵ_M and ϵ_D are the relative permittivity for metal and surrounding dielectric materials. We retain only the $l = 1$ spherical harmonics and consider only a particle radius r_0 , such that $r_0 \ll \lambda$ (i.e. the dipole limit). Note that the plasmon polariton frequency is resonant when $Re\{\epsilon_M(\omega)\} + 2\epsilon_D(\omega) \approx 0$, which for a Au particles is at $\lambda \sim 500\text{nm}$. However, the strong ohmic loss in the vicinity of this wavelength reduces the overall fluorescence enhancement.

Now consider the simplest multiparticle ensemble, namely a dimer of two spherical nanoparticles. Our TCM calculations show that coupling between the two Au nanoparticles changes their optical properties including a strong field enhancement and a down-shifting of the plasmon resonant frequency of the assembly, compared to the response of a single metal nanosphere. For a single Au spherical particle, the strongest enhancement occurs at 520nm [10], but for the Au dimer structure, the peak enhancement is, say, red shifted to 570nm (for a spherical-dimer with radius of 40nm), due to the lower plasmon resonant frequency. With this geometry, the enhanced intensity decreases as the spacing increases, which is demonstrated by the dashed line

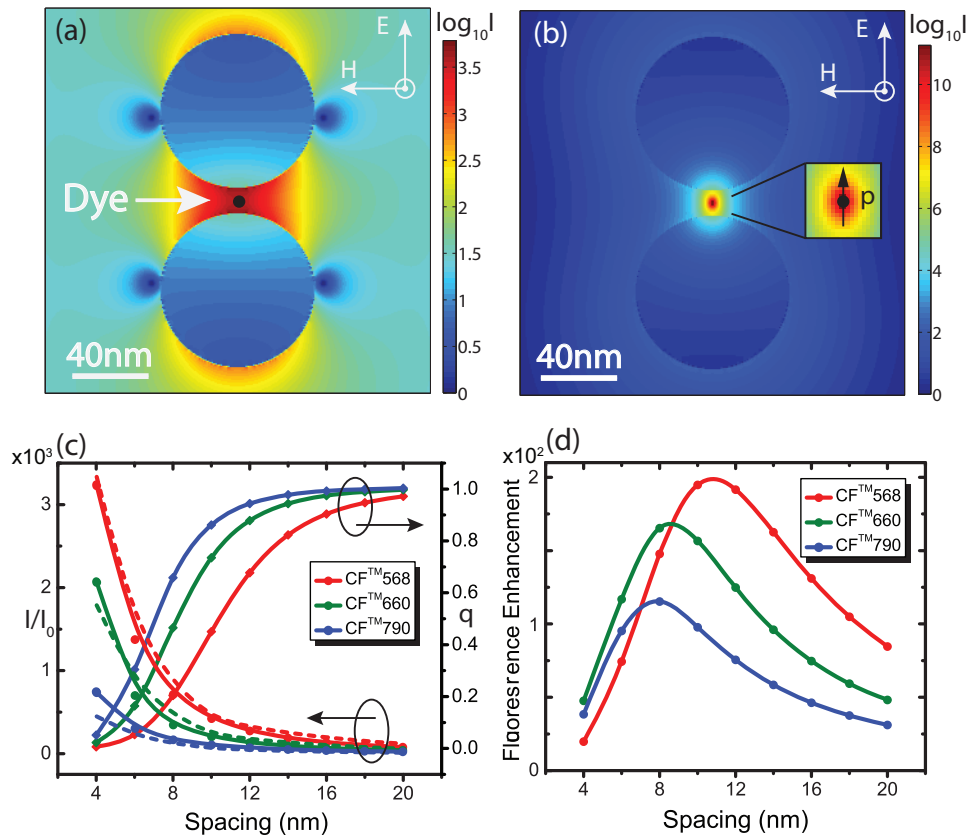


Fig. 4. (a) Plot of the intensity distribution of a dye/dimer complex under illumination by a *cw* source at the maximum absorption frequency of dye molecules, i.e. 562nm. (b) The intensity distribution for an excited dye molecule at its maximum emission frequency, i.e. 583nm. (c) A comparison of calculations of excitation rate $\gamma_{exc}/\gamma_{exc}^0$ using TCM theory (dashed lines) with calculated curves using FDTD (solid lines) for three dye molecules. Also, the FDTD calculated the quantum yield q as a function of dimer separation for different spacing. (d) The calculated emission rate $\gamma_{em}/\gamma_{em}^0$ and as a function of dimer separation for different particle sizes.

shown in Fig. 4(c). Further, our TCM results show that this new spectral response, in turn, leads to less ohmic loss. Note that this red-shifting has been previously introduced and reported in [35, 36] and this prior work on this model system was used to provide a validation of our model. Our TCM calculations show that the size of the Au nanospheres and the distance between their centers directly controls the magnitude of the red shift of the resonant wavelengths, a result also shown in prior work [16].

Finally, we add a cautionary note. Recently Nordlander [37] and Pendry [38] have studied quantum phenomena that occur when the surfaces of two Au particles are within sub-nanometer distances of each other. However, this near-contact case is not the focus of our research here. Instead, we examine cases, in which the Au particles are separated by a surface-to-surface spacing, which is larger than 4nm. Therefore, the small near-contact effects, such as quantum tunneling, are ignored in our calculations.

Numerical computation of enhancement and spectral shifts. Consider now our FDTD computations. The intensity enhancement obtained when illuminating with a *cw* source at the max-

imum absorption frequency of a dye molecule and in the presence of a dimer antenna is shown in Fig. 4(a); in this figure the dye molecule is located at the center of the spacing between the two spheres of the dimer. In addition, the incident field is, as shown, polarized parallel to the dimer axis. The numerical results of the antenna intensity enhancement at the location of dye molecule with respect to the spacing between sphere particles are demonstrated in Fig. 4(c). Recall that in this paper, in order to compare the dye/antenna assemblies uniformly, we fixed the volume of Au in the dimer to be equal to that in a spherical antenna with a radius of 40nm, in which case, the spherical antenna has a plasmon resonant frequency that is peaked near the maximum excitation wavelength of $CF^{TM}568$. The fluorescence quenching, due to the ohmic losses of the dye/nanoantennae assemblies, has also been investigated. By treating the excited dye molecule as a dipole source (see Fig. 4b), we find that the dipole radiative decay rate is related to its surrounding environment and the non-radiative decay rate is proportional to the power absorbed by the Au particles; this dependence enables us to calculate the quantum yield for different dye molecules and dimer antennae of different dimensions. Figure 4(c) shows the overall quantum yield, q , for our three different dye molecules. As the spacing is reduced, the in-coupling coefficient from the radiating dye molecule to the Au particles increases. In particular, more of the optical energy emitted from each dye molecule is then dissipated through ohmic losses in the Au-particle antenna, thus causing a decreased quantum yield. As shown in Eq. (1), the total fluorescence enhancement reflects the combined effects of excitation and quenching. In summary, for the aforementioned three dye molecules, we can achieve a 100-200 fluorescence enhancement by using spacings of 8-11.5nm. A plot of the performance of each dye/antenna type is given in Fig. 4(d).

Finally, as discussed in the previous section, standard TCM underestimates the antenna-intensity enhancement, especially when the interparticle spacing in the dimer is very small ($<10\text{nm}$). This underestimate is due to the fact that the isolated-sphere solution is used to calculate the overlap integral for intersphere coupling. In effect, this approach assumes that the polarizability α of each particle behaves as it would for an isolated particle, which in turn affects the value of γ_{rad} . We note, however, at such close spacing, we can treat the dimer pair as a single-dipole with an increased polarizability α_{pair} , due to the coupling between the original dipole moments of the spheres; this effect has been described in [7]. When this approach is used in the TCM framework, the results, as shown in Fig. 4(c) (dashed line), are in good agreement with our FDTD calculations.

4.2. Ellipsoid dimer

In the previous section, it was shown that a spherical-dimer nanoantenna is well matched for enhancing the fluorescence efficiency of a $CF^{TM}568$ dye. To enhance fluorescence for a longer wavelength dye, such as $CF^{TM}660R$, the spherical shape was changed into an ellipsoid; the longer major axis of ellipsoid nanoantenna was adjusted to match the plasmon resonance of the structure with the longer-wavelength emission peak of dye molecules, i.e., 663nm. This approach is based on insight from our TCM solution, which suggests that an ellipsoidal structure will yield a larger polarizability and stronger coupling coefficient at longer wavelength, thus allowing us to increase the intensity $|a|^2/|s_+|^2$. Hence, in this section, we use ellipsoid dimers and, for simplification, focus on spheroids, which have two axes of equal length; therefore, only one geometrical factor is independent. From our results on spherical dimers, we recall that the dimer structure has $200\times$ the fluorescence enhancement for $CF^{TM}568$ compared with its value for the molecule with no antenna, while the enhancement for $CF^{TM}660R$ is only $150\times$ and only $100\times$ for $CF^{TM}790$. The low values for the last two dyes is due to the fact these wavelengths are off-resonance for their emission wavelengths, as was shown in a notional way in Fig. 1. Thus we can achieve better fluorescence enhancement for dye molecules, simply by altering

the shape of the nanoantennae to change its LSP mode.

Figure 5(a) shows the intensity distribution of a spheroid dimer under illumination by a *cw* source at the wavelength of maximum absorption for three dye molecules. In addition, for this figure, the major axis is aligned along the polarized E-field of incident light. The polarizability, α , of an isolated spheroid in a field parallel to its major axis is then

$$\alpha = 4\pi abc \frac{\epsilon_M - \epsilon_D}{3\epsilon_D + 3L(\epsilon_M - \epsilon_D)} \quad (11)$$

where a is its major axis and $b = c$ are its minor axes; ϵ_M and ϵ_D are the dielectric constants of the metal and the surrounding medium. An analytical expression for the geometrical factor L as a function of the eccentricity $e = \sqrt{1 - b^2/a^2}$ can then be found from [39]:

$$L = \frac{1 - e^2}{e^2} \left(-1 + \frac{1}{2e} \ln \frac{1 + e}{1 - e} \right) \quad (12)$$

Based on Eqs. (11), (12) and setting $a > b = c$, the choice of a longer major axis a will yield a smaller L , which will lead to stronger polarizability α . Based on the quasi-static approximation, the near-field enhancement of such a spheroid, in general, will be much larger than that of a sphere of comparable volume. In fact this high enhancement is obtained in our calculation, as shown in Fig. 5(b). This result can also be seen from application of the TCM solution. In particular, since the spheroid's radiative mode is more directional than that of a sphere, the coupling coefficient κ for the spheroidal dimer is also larger. Based on Eq. (8), the magnitude of a/s_+ will increase when κ is increased. In our simulations, our spheroid antenna was designed

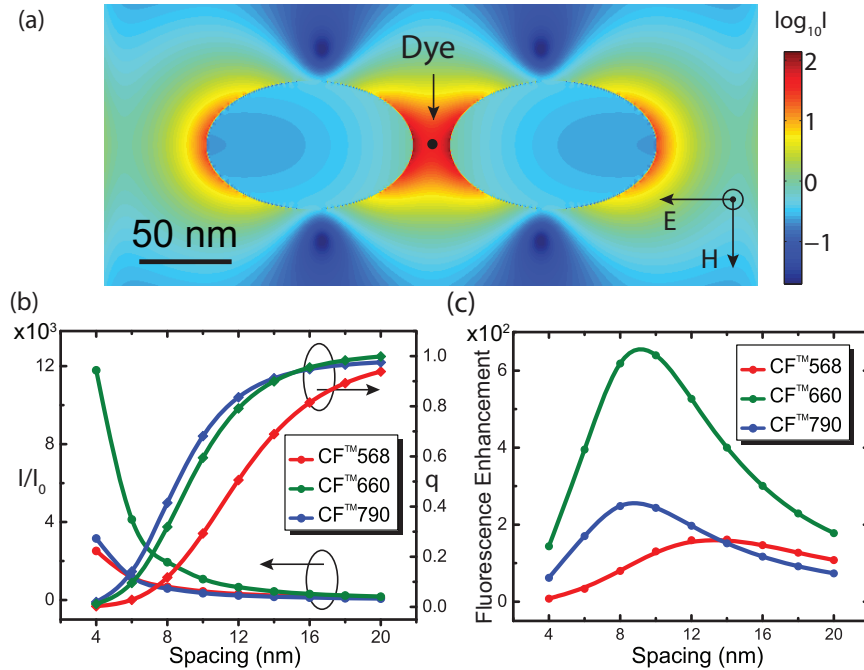


Fig. 5. (a) The intensity distribution under illumination from a *cw* source, having the absorption wavelength of a specific dye molecule. (b) Calculated excitation rate, $\gamma_{exc}/\gamma_{exc}^0$, and quantum yield, q , as a function of dimer separation. (c) Calculated emission rate, $\gamma_{em}/\gamma_{em}^0$, as a function of dimer separation.

to be $a = 110.7\text{nm}$ and $b = c = 34\text{nm}$, since these dimensions yield a resonant frequency of 665nm . As shown in Fig. 5(c), this antenna structure has a $650\times$ fluorescence enhancement for $CF^{TM}660R$ when the surface-to-surface spacing is 8nm . This result is more than $4\times$ than for a spherical-dimer antenna. For $CF^{TM}790$, the spheroid still has a $250\times$ fluorescence enhancement - that is $3\times$ times higher than that obtained when using a sphere. It is worth noting that a recent publication has reported an advanced fabrication capability that can synthesize a cylinder nanorod with round tip [40]. However, for our equivolume design rule, the cylinder dimer normally resonates in the near-IR spectrum that is out of the range of commercial dye-molecule fluorescence. The fluorescence enhancement is thus very weak at our three selected dye wavelengths using a cylinder dimer and thus its use will not be discussed further here.

4.3. Bowtie

In order to *efficiently* fluoresce at the longest wavelength considered in this paper, it was necessary to consider and examine a third dimer structure - the nanobowtie (triangle dimer). Using the same approach, the fluorescence enhancement of a bowtie nanoantenna was investigated, again with the same fixed volume of Au as was used for the spherical dimer discussed above. The choice of a bowtie to increase fluorescence enhancement at longer wavelengths was also motivated by the TCM theory. In particular, its strong near-field coupling and its large planar area cause it to have a stronger resonance at a longer wavelength than for the two antennae discussed above. Note also that its use has also been enabled by a recent development in advanced fabrication procedures [41, 42].

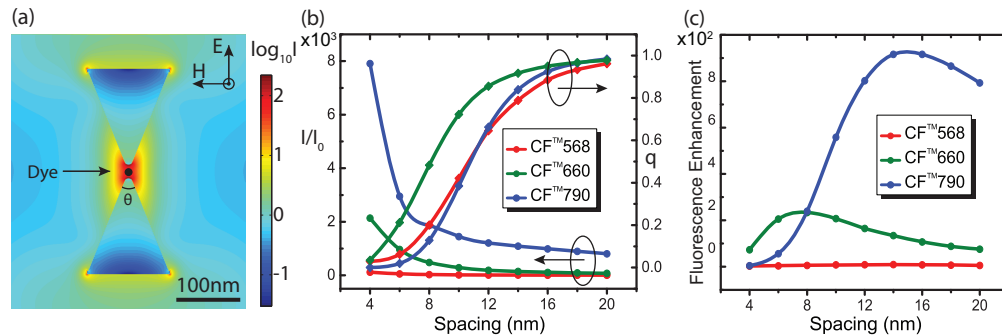


Fig. 6. (a) The intensity distribution, I , due to the illumination of a *cw* source at the maximum absorption wavelength of the three dye molecules. (b) Calculated excitation rate, $\gamma_{exc}/\gamma_{exc}^0$, and quantum yield, q , as a function of dimer separation. (c) Calculated emission rate $\gamma_{em}/\gamma_{em}^0$ and as a function of dimer separation for different particle sizes.

The bowtie has several features, which are qualitatively distinct from those of our other two nanodimers. One of these is its sharp point, which leads to a high directionality radiation. The second difference is that, for a fixed nanoparticle volume, the bowtie has a higher in-coupling coefficient κ_{in} and is resonant at longer wavelengths than for ellipsoids and spherical dimers. Based on Eq. (8); this high directionality in-coupling coefficient, κ , will further increase the field enhancement.

The intensity enhancement resulting from normal-incidence light impinging on a bowtie structure is shown in Fig. 6(a). Using our optimization procedure to scan through bowtie configurations with thicknesses from 20 to 40nm and angle θ from 30° to 120° , we find a local optimal enhancement structure of 30nm-thickness with a width of 120nm and a height of 149nm. As anticipated, the bowtie has a much stronger resonance at 800nm wavelength than at 560nm as indicated in Fig. 6(b). Although the quantum yield of the bowtie structure is comparable to that

of the spherical dimers, the field enhancement of the bowtie dimer is stronger. From Fig. 6(c), we see that the optimal spacing between the bowtie tips for a $CF^{TM}790$ molecule is 14nm, which gives a $900\times$ fluorescence enhancement compared with $150\times$ fluorescence enhancement with a spherical dimer structure and $300\times$ fluorescence enhancement with an ellipsoidal dimer. The enhancement for a $CF^{TM}660R$ dye using a bowtie dimer structure is comparable to that achieved with a spherical-dimer antenna, however as expected, the enhancement for a $CF^{TM}568$ dye is significantly weaker. In summary, the bowtie structure is well matched to the near-IR fluorescent molecule.

5. Conclusion

In order to summarize our theoretical investigation of our three different choices of nanoantennae, we present our optimal fluorescence enhancement data for each configuration for the dye-molecules $CF^{TM}568$, $CF^{TM}660R$ and $CF^{TM}790$ in Table 1. As the table shows, there is an optimal antenna structure for high fluorescence enhancement for each specific dye-molecule pair; this enhancement is due to the different plasmonic response and field coupling with variation in shape at each wavelength. Our results show that, guided by TCM analysis, use of 3D FDTD computation of enhancement and metallic loss can provide accurate fluorescence enhancement calculations for arbitrary-shaped metal nanoparticle antennae. These results enable rational design of metallic nanoparticle complexes for maximum fluorescence enhancement. Thus with the help of our theoretical tools, it is possible to design assemblies before synthesis and fabrication procedures, so as to achieve high performance. As computing hardware architecture advances, this method will soon be able to be implemented on a single desktop server with massively parallel processors and extensive memory.

Table 1. Summary of the maximum fluorescence enhancement for each dye molecules

	Max. Fluorescence Enhancement		
	$CF^{TM}568$	$CF^{TM}660R$	$CF^{TM}790$
Sphere	200	170	115
Ellipsoid	160	650	250
Bowtie	10	235	920

Acknowledgments

We thank Oleg Gang and Matthew Sfeir for their insightful discussions regarding Au nanoparticle assemblies as well as Mark Hybersten and Deyu Lu for their assistance in adapting the simulation software for use on a computer cluster. We also thank James Misewich, Nathaniel Osgood and Richard Osgood (III) for helpful discussion during the research. The simulations were performed on the computer cluster in the Center for Functional Nanomaterials (CFN) at the Brookhaven National Laboratory (BNL), which is supported by the U.S. Department of Energy, Office of Basic Energy Sciences, under Contract No. DE-AC02-98CH10886. The research described here is based upon work supported as part of the Center for Re-Defining Photovoltaic Efficiency through Molecule Scale Control, an Energy Frontier Research Center funded by the U.S. Department of Energy, Office of Science, Office of Basic Energy Sciences under Award Number DESC0001085. We also thank the support from Wei Family Private Foundation in helping X.M. attending professional meetings related to this research. N.C.P. was supported by EPSRC, grant No. EP/J018473/1.